Inorganic Chemistry

Article

pubs.acs.org/IC

Dispersion Force Stabilized Two-Coordinate Transition Metal−Amido Complexes of the −N(SiMe$_3$)Dipp (Dipp = C$_6$H$_3$-2,6-Pr$^i_2$) Ligand: Structural, Spectroscopic, Magnetic, and Computational Studies

Chun-Yi Lin,[†] Jing-Dong Guo,[‡] James C. Fettinger,[†] Shigeru Nagase,*[,‡] Fernande Grandjean,[§] Gary J. Long,*[,§] Nicholas F. Chilton,[⊥] and Philip P. Power*[,†]

[†]Department of Chemistry, University of California, Davis, California 95616, United States

[‡]Fukui Institute for Fundamental Chemistry, Kyoto University, 34-4 Takano-Nishihiraki-cho, Sakyou-ku, Kyoto 606-8103, Japan

[§]Department of Chemistry, Missouri University of Science and Technology, University of Missouri, Rolla, Missouri 65409-0010, United States

[⊥]School of Chemistry, University of Manchester, Oxford Road, Manchester M13 9PL, United Kingdom

Supporting Information

ABSTRACT: A series of high spin, two-coordinate first row transition metal−amido complexes, M{N(SiMe$_3$)Dipp}$_2$ {M = Fe (**1**), Co (**2**), or Ni (**3**); Dipp = C$_6$H$_3$-2,6-Pr$^i_2$} and a tetranuclear C−H activated chromium amide, [Cr{N(SiMe$_2$CH$_2$)-Dipp}$_2$Cr]$_2$(THF) (**4**), were synthesized by reaction of their respective metal dihalides with 2 equiv of the lithium amide salt. They were characterized by X-ray crystallography, electronic and infrared spectroscopy, SQUID magnetic measurements, and computational methods. Contrary to steric considerations, the structures of **1**−**3** display planar eclipsed M{NSiC(ipso)}$_2$ arrays and short M−N distances. DFT calculations, corrected for dispersion effects, show that dispersion interactions involving C−H−H−C moieties likely stabilize the structures by 21.1−29.4 kcal mol^{-1}, depending on the level of the calculations employed. SQUID measurements confirm high spin electron configurations for all the complexes and substantial orbital contributions for **1** and **2**.

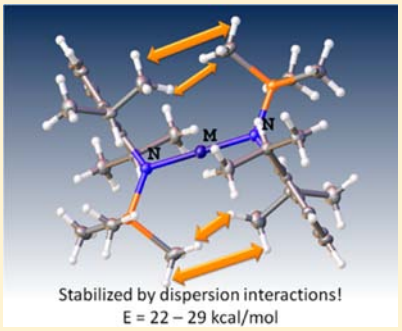

INTRODUCTION

Several recent publications on two-coordinate, open-shell (d^1−d^9) transition metal complexes have shown that they have unusual magnetic properties. For example, two-coordinate iron(II) complexes such as Fe{C(SiMe$_3$)$_3$}$_2$,[1−3] Fe(NBu$^t_2$)$_2$,[4] or Fe{N(H)Ar$^{Pr^i_6}$}$_2$ (Ar$^{Pr^i_6}$ = C$_6$H$_3$-2,6(C$_6$H$_2$-2,4,6-Pr$^i_3$)$_2$)[5] have magnetic moments far in excess of the spin-only value μ_{SO} = 4.9μ_B, and can approach the free ion magnetic moment of 6.7μ_B. In essence, the first-order orbital angular momentum (OAM) in these iron(II) (S = 2) complexes remains unquenched because both ligands are bound along only one axis (z), so that electron circulation in the unequally occupied, degenerate $d_{x^2-y^2}$ and d_{xy} orbitals, which cause the orbital moment, remains unimpaired. Very high magnetic moments have also been observed in the linear coordinated cobalt complex Co{N(H)Ar$^{Pr^i_6}$}$_2$ (S = 3/2, μ_{eff} = 6.3μ_B),[6a] which is thought to be due to out of state spin orbit coupling. In contrast, in their nickel analogue Ni{N(H)Ar$^{Pr^i_6}$}$_2$,[6a] where first-order effects are also expected due to unequally occupied d_{xz} and d_{yz} orbitals, a magnetic moment of only 2.92μ_B was measured, which is just slightly higher than the expected spin-only value of 2.83μ_B. The closely related, linear nickel(II) derivative Ni{N(H)Ar$^{Pr^i_4}$}$_2$ (Ar$^{Pr^i_4}$ = C$_6$H$_3$-2,6(C$_6$H$_3$-2,6-Pr$^i_2$)$_2$) also had a magnetic moment (2.79μ_B) near that of the spin only value.[6b] Their linear chromium analogue Cr{N(H)Ar$^{Pr^i_6}$}$_2$ (d^4, S = 2)[7] had μ_{eff} = 4.22μ_B, which is lower than the expected spin-only value of 4.9μ_B. This is consistent with the positive value of the spin−orbit coupling constant for the less than half-filled valence shell. Further experiments with closely related, less-crowded complexes of formula M{N(H)Ar^{Me_6}}$_2$,[5,6a,7] which generally have bent coordination geometries, have shown that the bending can result in drastic changes to their magnetic moments, owing to a lifting of orbital degeneracy and consequent quenching of the first-order OAM.

These experiments have demonstrated that the geometries of the two-coordinate species are of key importance and that linear or near-linear geometries are highly desirable to maximize orbital magnetic moment effects. Furthermore, linear coordination provides a highly anisotropic metal environment that may generate highly negative axial zero-field splittings,[8,9] as well as increased barriers to spin reversal.[10,11] Yet, two-coordinate complexes with linear geometries in the crystalline state form a relatively small minority (ca. 12) of the ca. 80 two-coordinate open-shell (d^1−d^9) transition metal complexes that are

Received: August 16, 2013
Published: November 18, 2013

 © 2013 American Chemical Society dx.doi.org/10.1021/ic402105m | Inorg. Chem. 2013, 52, 13584−13593

Table 1. Selected Crystallographic Data and Collection Parameters for 1−4

	1	2	3	4
formula	$C_{30}H_{52}FeN_2Si_2$	$C_{30}H_{52}CoN_2Si_2$	$C_{30}H_{52}NiN_2Si_2$	$C_{64}H_{108}Cr_4N_4OSi_4$
fw, g mol^{-1}	552.77	555.84	555.63	1269.90
habit	block	block	block	block
color	orange	dark red	purple	green
cryst syst	triclinic	triclinic	triclinic	monoclinic
space group	$P\bar{1}$	$P\bar{1}$	$P\bar{1}$	$P2_1/c$
a, Å	8.8101(5)	8.8518(10)	8.9104(13)	10.2421(3)
b, Å	9.1759(5)	9.1815(10)	9.1955(13)	16.2208(5)
c, Å	11.1624(6)	11.0926(11)	10.9978(16)	40.7752 (13)
α (deg)	102.4670(10)	102.5194(14)	102.065(2)	90
β (deg)	92.5030(10)	92.4082(14)	92.547(2)	94.5098(13)
γ (deg)	113.9320(10)	114.0167(13)	114.364(2)	90
V, Å^3	796.59(8)	795.28(15)	794.0(2)	6753.2(4)
Z	1	1	1	4
d_c, Mg m^{-3}	1.152	1.161	1.162	1.249
θ range (deg)	1.89−27.51	1.90−32.40	1.91−29.21	3.486−70.077
μ, mm^{-1}	0.568	0.635	0.706	6.154
obs data, $I > 2\sigma(I)$	3336	3520	3824	12 369
R_1 (obs data)	0.0378	0.0357	0.0265	0.0426
wR_2 (all data)	0.1073	0.1065	0.0753	0.1073

currently known.[12a,b] It is clear that exceptionally large ligand substituents are required to ensure linear coordination at the metals in the crystalline phase.[13] The use of the $-C(SiMe_3)_3$ alkyl group allowed the isolation of the first two-coordinate open-shell transition metal species $Mn\{C(SiMe_3)_3\}_2$[14] in the solid state, but until now this ligand has been demonstrated to stabilize two coordination for one other metal: in the iron species $Fe\{C(SiMe_3)_3\}_2$[1−3] and in the recently described salt $[K(crypt\text{-}222)][Fe\{C(SiMe_3)_3\}_2]$.[11] Most of the other examples of strictly linearly coordinated Cr−Ni metal complexes feature the terphenyl-substituted amido and thiolato ligands $-N(H)Ar^{Pr^i_6}$[5−7] and $-SAr^{Pr^i_6}$ ($Ar^{Pr^i_6}$ = C_6H_3-2,6(C_6H_2-2,4,6-Pr^i_3)$_2$).[15] However, these ligands, although effective, have the disadvantage that they require time-consuming syntheses. We turned to the more easily synthesized $-N(SiMe_3)Dipp$ (Dipp = C_6H_3-2,6-Pr^i_2) ligand of Wigley[16] (which has also been shown to stabilize two-coordination in the magnesium, zinc, and mercury derivatives $M'\{N(SiMe_3)Dipp\}_2$,[16b,c] M′ = Mg, Zn, Hg), to isolate a series of two-coordinate complexes, $M\{N(SiMe_3)Dipp\}_2$ (M = Fe, **1**; Co, **2**; Ni, **3**), which we describe in full here. We show that these complexes have rigorously linear coordination in the solid state, with unusual extended planar $M\{NSi(C(ipso))\}_2$ core arrays and short M−N distances. We also show that attempts to synthesize the corresponding Cr^{2+} derivative afforded a further reaction involving a C−H moiety from a $SiMe_3$ group of the ligands, which yielded the unusual tetrametallic complex $[Cr\{N(SiMe_2CH_2)Dipp\}_2Cr]_2(THF)$ (**4**). We had earlier given the M−N distances and N−M−N bond angles for **1**−**3** in a review,[12a] and while their characterization was still in progress, the synthesis, structure, and several reactions of $Ni\{N(SiMe_3)Dipp\}_2$[17] were reported by Tilley and co-workers. As a part of a collaborative effort, we also described some magnetic properties of $Fe\{N(SiMe_3)Dipp\}_2$ as part of a larger study involving the magnetic relaxation of two coordinate iron(II) species.[10] Here, we describe a more detailed study of the spectroscopic and magnetic properties of compounds **1**−**4** and describe their electronic structure and bonding through a combination of spectroscopic and computational methods. Moreover, we show that attractive dispersion forces between the ligand across the metal likely play a key role in stabilizing their structures with energies in the range *ca.* 21.1−29.4 kcal mol^{-1} being calculated.

EXPERIMENTAL SECTION

General Methods. All manipulations were carried out by using modified Schlenk techniques under an atmosphere of N_2 or in a Vacuum Atmospheres HE-43 drybox. All solvents were dried over an alumina column, followed by storage over 3 Å molecular sieves overnight, and degassed three times (freeze−pump−thaw) prior to use. Anhydrous $FeCl_2$ was obtained by heating $FeCl_2{\cdot}4H_2O$ to 150 °C under vacuum for 18 h. $CoCl_2$ was purchased from Strem Chemicals Inc. and was used as received. The compounds $LiN(SiMe_3)Dipp$[18] (Dipp = C_6H_3-2,6-Pr^i_2), $CrCl_2(THF)_2$,[19] and $NiCl_2(DME)$[20] (DME = 1, 2-dimethoxyethane) were prepared according to literature procedures. Melting points were measured in glass capillaries sealed under N_2 by using a Mel-Temp II apparatus and are uncorrected. UV−vis spectra were collected using an Ocean Optics DH2000 light source and HR2000 CG-UVNIR spectrometer.

$Fe\{N(SiMe_3)Dipp\}_2$ (1). $LiN(SiMe_3)Dipp$ (3.0078 g, 11.78 mmol) was dissolved in 50 mL of Et_2O, and the solution was added dropwise to a suspension of $FeCl_2$ (0.712 g, 5.62 mmol) in Et_2O (10 mL) with cooling to ca. 0 °C. The dark brown reaction mixture was allowed to warm to room temperature and was stirred for 18 h. All volatile materials were removed under vacuum, and the residue was extracted with hexanes (40 mL). The solution was filtered, and the dark brown filtrate was concentrated to incipient crystallization. Storage at ca. −18 °C overnight afforded large, X-ray quality orange crystals of **1**. Yield: 1.7836 g (57.5%). Mp: 209−211 °C. UV−vis (hexane) λ_{max} (ε): 344 nm (6200 mol^{-1} L cm^{-1}).

$Co\{N(SiMe_3)Dipp\}_2$ (2). $LiN(SiMe_3)Dipp$ (1.4669 g, 5.74 mmol) was dissolved in Et_2O (50 mL) and added dropwise to $CoCl_2$ (0.3425 g, 2.64 mmol) at ca. 0 °C with rapid stirring. The dark red reaction mixture was allowed to warm to room temperature and stirred for 18 h. All volatile materials were removed under vacuum, and the residue was extracted with hexanes (40 mL). The solution was filtered, and the dark red filtrate was concentrated to incipient crystallization. Storage at ca. −18 °C overnight afforded large, X-ray quality dark red crystals. Yield: 1.1252 g (76.8%). Mp: 177−180 °C. UV−vis (hexane) λ_{max} (ε): 504 nm (470 mol^{-1} L cm^{-1}). Anal. Calcd for $C_{30}H_{52}CoN_2Si_2$: C, 64.82; H, 9.43; N, 5.04. Found: C, 65.08; H, 9.51; N, 4.96.

$Ni\{N(SiMe_3)Dipp\}_2$ (3). $LiN(SiMe_3)Dipp$ (1.5131 g, 5.92 mmol) was dissolved in 50 mL of Et_2O and slowly added to 0.6182 g (2.81

dx.doi.org/10.1021/ic402105m | Inorg. Chem. 2013, 52, 13584−13593

mmol) of $NiCl_2$(DME) at ca. 0 °C. The purple reaction mixture was allowed to warm to room temperature and stirred for 18 h. All volatile material was removed under vacuum, and the residue was extracted with hexanes (40 mL). The solution was filtered, and the dark purple filtrate was concentrated to incipient crystallization. Storage at ca. −18 °C for several days afforded X-ray quality dark purple crystals. Yield: 0.3899 g (24.9%). Mp: 163−165 °C. UV−vis (hexane) λ_{max} (ε): 508 nm (5600 mol^{-1} L cm^{-1}). Anal. Calcd for $C_{30}H_{52}NiN_2Si_2$: C, 64.85; H, 9.43; N, 5.04. Found: C, 65.19; H, 9.30; N, 4.99.

[Cr{N(SiMe$_2$CH$_2$)Dipp}$_2$Cr]$_2$(THF) (4). LiN(SiMe$_3$)Dipp (2.1048 g, 8.24 mmol) was dissolved in 50 mL of Et_2O and slowly added to 1.1058 g (3.80 mmol) of $CrCl_2(THF)_2$ at ca. 0 °C. The dark green reaction mixture was allowed to warm to room temperature. After 2 days of stirring, all volatile material was removed under reduced pressure, and the residue was extracted with pentane. The solution was filtered, and the deep green filtrate was concentrated to incipient crystallization. Storage at ca. − 18 °C for several days afforded X-ray quality deep green crystals. Yield: 0.3968 g (31.6%). UV−vis (hexane) λ_{max} (ε): 366 (3700), 468 (1000) nm (mol^{-1} L cm^{-1}). Anal. Calcd for $C_{64}H_{108}Cr_4N_4OSi_4$: C, 60.53; H, 8.57; N, 4.41. Found: C, 60.01; H, 8.19; N, 4.16.

X-ray Crystallography. Crystals of **1**−**4** were removed from a Schlenk flask under a stream of nitrogen and immediately covered with a layer of hydrocarbon oil. A suitable crystal was selected, attached to a glass fiber on a copper pin, and quickly placed in the cold N_2 stream on the diffractometer. Data for compound **2** were collected at *ca.* 90 K on a Bruker SMART 1000 diffractometer with Mo Kα radiation (λ = 0.710 73 Å). Data for compounds **1**, **3**, and **4** were collected at 90 K on a Bruker APEX DUO diffractometer with Mo Kα radiation (λ = 0.710 73 Å). Absorption corrections were applied using SADABS.[21] The crystal structures were solved by direct methods and refined by full-matrix least-squares procedures in SHELXTL.[22] All non-H atoms were refined anisotropically. All H atoms were placed at calculated positions and included in the refinement using a riding model.

Data collection parameters and a summary of the structural refinements are given in Table 1.

Magnetic Studies. The powdered samples of **1**−**4** used for magnetic measurements were sealed under N_2 in 3 mm diameter quartz tubing. The sample magnetization was measured using a Quantum Design MPMSXL7 superconducting quantum interference magnetometer. For each compound, the sample was zero-field cooled to 2 or 5 K and the long moment was measured upon warming to 320 K in an applied field of 0.01 T. To ensure thermal equilibrium between the powdered sample in the quartz tube and the temperature sensor, the long moment at each temperature was measured after 50, 36, 28, 20, and 12 min intervals over the temperature ranges of 2−6, 6−10, 10−25, 25−70, and 70−320 K, respectively; the measurements required ca. 20 h for each sample. Diamagnetic corrections of −0.000353, −0.000352, −0.000351, and −0.000851 emu/mol, obtained from tables of Pascal's constants,[23] were applied to the measured susceptibility of **1**−**4**, respectively.

Computational Methods. All calculations were carried out using the Gaussian program.[24] Geometry optimization was performed with hybrid density functional theory (DFT) at the spin-unrestricted B3PW91 level, by using the 6-311+G* basis set for Fe, Co, and Ni and the 6-31G(d) basis set for other atoms. The harmonic vibrational frequencies and infrared intensities of optimized geometries were also calculated. The UV/vis absorption spectra of optimized geometries were calculated using the time dependent (TD) B3PW91 method. In order to estimate the dispersion effects, these complexes were reoptimized with the dispersion-corrected B3PW91-D3 functional.[25a] The performance of another dispersion-corrected GGA functional, B97D, was also explored and compared with that of the higher-level B3PW91-D3 treatment.

To account for basis set superposition error (BSSE),[25b] the correction was estimated with the complex **3** as an example. It was found that this error is smaller than 5 kcal/mol in the bond dissociation energy (BDE) but only 0.7 kcal/mol in the dispersion energy given in Table 6, suggesting that the correction can be neglected to the dispersion term.

RESULTS AND DISCUSSION

Synthesis and Structure. The complexes **1**−**3** were synthesized in moderate yields by a transmetalation approach that involved the treatment of $FeCl_2$, $CoCl_2$, and $NiCl_2$(DME) with 2 equiv of LiN(SiMe$_3$)Dipp in Et_2O at ca. 0 °C (Scheme 1).

Scheme 1. Synthesis of 1, 2, and 3

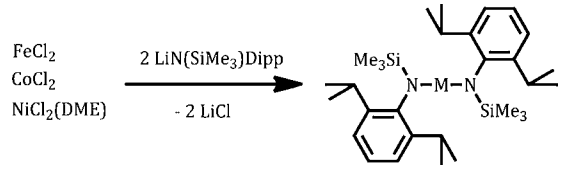

Workup was straightforward and involved extraction of the reaction mixture residue with hexanes and filtration to remove lithium chloride. Recrystallization of the deeply colored solutions of **1**−**3** afforded crystals that were suitable for X-ray crystallography.

The thermal stability of compounds **1**−**3** is noteworthy, especially that of **3** where the related −N(SiMe$_3$)$_2$ derivative, Ni{N(SiMe$_3$)$_2$}$_2$,[26] was found to decompose at room temperature. In contrast, the corresponding manganese, iron, and cobalt M{N(SiMe$_3$)$_2$}$_2$ (M = Mn,[26] Fe,[27] or Co[28]) species are thermally stable and can be distilled under reduced pressure at temperatures >100 °C. It appears that the use of aryl substituents at nitrogen in nickel amides confers increased stability, as evidenced by the stable homoleptic Ni(II) monomers Ni{N(H)Ar^{Me_6}}$_2$ (Ar^{Me_6} = C$_6$H$_3$-2,6(C$_6$H$_2$-2,4,6-Me$_3$)$_2$),[6a] Ni{N(H)Ar$^{Pr^i_4}$}$_2$,[6b] Ni{N(H)Ar$^{Pr^i_6}$}$_2$,[6a] Ni{N(Ph)B(Mes)$_2$}$_2$ (Mes = C$_6$H$_2$-2,4,6-Me$_3$),[29] Ni{N(Mes)B(Mes)$_2$}$_2$,[30] the dimeric {Ni(NPh$_2$)$_2$}$_2$,[31] or the Ni(I) complex {CHN(Dipp)}$_2$Ni{N(H)Dipp}.[32] Within limits, therefore, the lack of stability does not appear to be due to insufficient steric protection, since bulkier silylamide ligands such as −N(SiMe$_2$Ph)$_2$ and −N(SiMePh$_2$)$_2$ can form stable two-coordinate manganese, iron, or cobalt complexes (see below, Table 3), but have not been shown to afford stable nickel(II) derivatives to date.[31,32]

The X-ray data showed that crystals of **1**−**3** are isomorphous, with very similar cell parameters (Table 1). Their structures consist of well-separated two-coordinate centrosymmetric monomers, as illustrated by the thermal ellipsoid plot of the cobalt derivative **2** in Figure 1. Selected structural parameters are given in Table 2.

The M−N distances decrease across the series M = Fe, Co, and Ni from 1.853(1) (Fe) to 1.818(1) (Co) to 1.8029(9) (Ni) Å (cf. Ni−N = 1.7987(11) Å in ref 17), consistent with decreasing element size. The closest metal−metal approaches are 8.8101(5) Å for **1**, 8.8493(7) Å for **2**, and 8.910.4(13) Å for **3**. The two most important features of the structures are the rigorously linear coordination of the metals, and the extended planar structure of the M{NSi(C$_{ipso}$)}$_2$ (C$_{ipso}$ = C(1)) core arrays, which have local C_{2h} symmetry. Strictly linear two coordination for open-shell transition metal complexes, which is important because of its effect on magnetic properties, is relatively rare in the solid state, and a total of nine such examples[3−7,11,14,15,35,36] had been characterized prior to the three −N(SiMe$_3$)Dipp derivatives. The extended planarity of the M{NSi(C$_{ipso}$)}$_2$ core is noteworthy because it may not represent a steric minimum (see below) for interactions

dx.doi.org/10.1021/ic402105m | Inorg. Chem. 2013, 52, 13584−13593

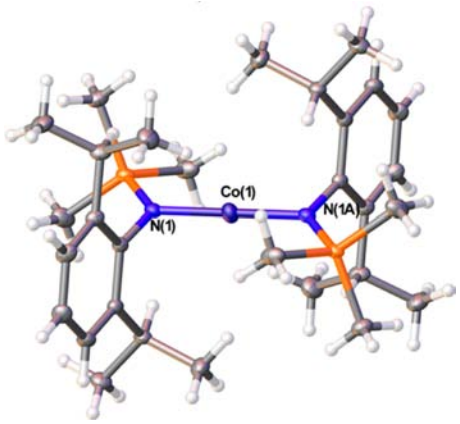

Figure 1. Solid state molecular structure of **2**. Thermal ellipsoids for non-H atoms are shown at 30% probability. See Table 2 for important bond lengths and angles.

Table 2. Important Interatomic Distances (Å) and Angles (deg) for Compounds 1−3

	1	2	3
M(1)−N(1)	1.8532(13)	1.8179(14)	1.8029(9)
N(1)−C(1)	1.4289(19)	1.4288(16)	1.4325(13)
N(1)−Si(1)	1.7261(14)	1.7305(11)	1.7417(10)
M(1)−C(1)	2.686(1)	2.650(1)	2.612(1)
N(1)−M(1)−N(1A)	180	180	180
M(1)−N(1)−C(1)	109.18(10)	108.71(8)	107.13(7)
M(1)−N(1)−Si(1)	125.08(8)	125.46(6)	126.02(5)
C(1)−N(1)−S(1)	125.74()	125.83()	126.85()

between $SiMe_3$ and Dipp substituents of the two amido groups across the metal. An examination of the structural data show that the $SiMe_3$−Pr^i H···H separations are only 2.43(1) Å (**1**, Fe), 2.37(1) Å (**2**, Co), and 2.36(1) Å (**3**, Ni), and each complex is stabilized by attractive dispersion forces (see below) between these moieties. Such forces have been shown by computational data to be of high importance in stabilizing a variety of structures with large substituents.[37−39] The M−N distances measured for each of the complexes are among the shortest known and are the shortest, in the case of **2** and **3**, for two-coordinate cobalt(II) or nickel(II) amido complexes (cf. Table 3). Prior to the $M\{N(SiMe_3)Dipp\}_2$ series, the transition metal compound most closely related stoichiometrically to **1**−**3** was the iron species $Fe\{N(CH_2Bu^t)Dipp\}_2$.[40] However, it does not have linear iron coordination, N−Fe−N = 168.8(2)°, although its Fe−N bond length, 1.842(2) Å, is marginally shorter than the 1.8532(13) Å in **1**. The closest nonbonded approaches of ligand atoms to the metal in **1**−**3** involve the *ipso*-carbon (C(1)) of the Dipp aryl ring at a distance of 2.686 Å (**1**), 2.650 Å (**2**), and 2.612 Å (**3**). These distances are comparable to the secondary M···C interactions observed in $M\{N(H)Ar^{Pr^i_6}\}_2$[5,6a] complexes of these metals, where Mössbauer studies[5] of the $Fe\{N(H)Ar^{Pr^i_6}\}_2$ indicate that the spectral parameters are consistent with two-coordination, implying that the M···C interactions are weak.

The use of less bulky $-N(SiMe_3)_2$ and $-NPh_2$ ligands on Fe, Co, and Ni results in dimerization through bridging by the amido ligands, $[(Me_3Si)_2NM\{\mu\text{-}N(SiMe_3)_2\}_2MN(SiMe_3)_2]$ (M = Mn,[41] Fe,[42] or Co[41b]) and $[Ph_2NM\{\mu\text{-}NPh_2\}_2MNPh_2]$ (M = Fe,[42] Co,[31] or Ni[31]) and an increase in the metal coordination number from 2 to 3.

Table 3. Comparison of M−N Bond Lengths of Two-Coordinate Fe(II), Co(II), and Ni(II) Diamido Complexes

complex	M−N (Å)	N−M−N (deg)	ref
$Fe\{N(CH_2Bu^t)Dipp\}_2$	1.842(2)	168.8(2)	40
1	1.8532(13)	180.0	this work
$Fe\{N(Bu^t)_2\}_2$	1.880(2)	179.45(8)	4
$Fe\{N(SiMe_2Ph)_2\}_2$	1.896(2)	172.1(1)	33, 34
$Fe\{NHAr^{Pr^i_6}\}_2$	1.902(1)	180.0	5
$Fe\{N(SiMePh_2)_2\}_2$	1.916(2)	169.0(1)	33
$Fe\{NHAr^{Me_6}\}_2$	1.909(3)	140.94(16)	5
$Fe\{N(Mes)B(Mes)_2\}_2$	1.938(2)	166.6(1)	30
2	1.8179(14)	180.0	this work
$Co(NHAr^{Me_6})_2$	1.836(11)	144.1(4)	6a
$Co(NHAr^{Pr^i_6})_2$	1.865(2)	180.0	6b
$Co\{N(SiMePh_2)_2\}_2$	1.898(3)	147.0(1)	33
$Co\{N(Mes)B(Mes)_2\}_2$	1.910(3)	168.4(1)	30
$Co\{N(Ph)B(Mes)_2\}_2$	1.909(5)	127.1(2)	30
3	1.8029(9)	180.0	this work
$Ni\{NHAr^{Pr^i_6}\}_2$	1.818(3)	180.0(3)	6b
$Ni\{NHAr^{Pr^i_6}\}_2$	1.8284(15)	180.0	6a
$Ni\{N(Mes)B(Mes)_2\}_2$	1.866(2)	167.9(1)	29
$Ni\{N(Ph)B(Mes)_2\}_2$	1.885(4)	135.7(1)	30

The chromium species **4** was obtained as dark green crystals from hexanes in moderate yield by treatment of $CrCl_2(THF)_2$ with 2 equiv of $LiN(SiMe_3)Dipp$ in an analogous manner to that used for **1**−**3**. The structure of **4** was solved by X-ray crystallography and shown to be the tetrametallic chromium-amido/alkyl complex, $[Cr\{N(SiMe_2CH_2)Dipp\}_2Cr]_2(THF)$ (Figure 2), in which the amido ligands have each been

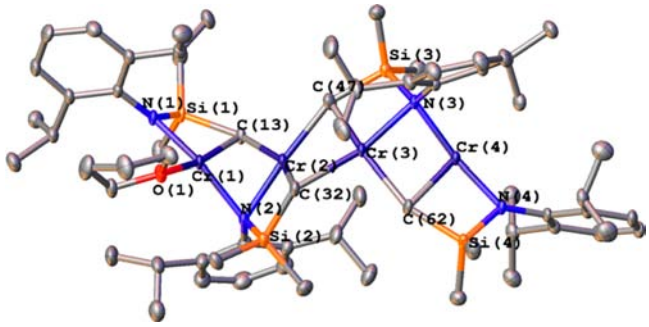

Figure 2. Solid state molecular structure of **4** (cf. Table 4 for details). H atoms are not shown for clarity, and thermal ellipsoids are shown at 30% probability.

dehydrogenated at one of the methyls attached to the silicon such that the ligand is in effect bidendate and carries a 2− charge. The dehydrogenation of methyl substituents in sterically crowded trimethylsilylamido derivatives of transition[43−47] (and other[48]) metals is well-known but is rare for chromium.[49]

Selected bond angles and distances for **4** are given in Table 4. Compound **4** exhibits an unusual tetrametallic structure, for which only a few related examples have been reported.[50,51] Of the four metals in the structure, the two outer chromiums, Cr(1) and Cr(4), are coordinated to two nitrogens, each from an amido ligand. One of these amido ligands bridges through its nitrogen to an inner chromium atom, while the other is terminally bound. Each outer chromium is also bonded to a

dx.doi.org/10.1021/ic402105m | Inorg. Chem. 2013, 52, 13584−13593

Table 4. Selected Bond Distances (Å) and Angles (deg) for 4

Cr(1)−N(1)	1.9894(14)	N(1)−Cr(1)−O(1)	93.50(7)
Cr(1)−N(2)	2.1236(19)	N(1)−Cr(1)−N(2)	158.13(8)
Cr(1)−O(1)	2.0848(16)	O(1)−Cr(1)−N(2)	100.32(7)
Cr(1)−C(13)	2.184(2)	N(1)−Cr(1)−C(13)	81.07(8)
Cr(2)−N(2)	2.062(19)	O(1)−Cr(1)−C(13)	167.98(8)
Cr(2)−C(13)	2.279(3)	N(2)−Cr(1)−C(13)	88.17(8)
Cr(2)−C(32)	2.210(3)	N(2)−Cr(2)−C(32)	79.94(8)
Cr(2)−C(47)	2.231 (3)	N(2)−Cr(2)−C(47)	175.57(9)
Cr(3)−N(3)	2.0805(18)	C(32)−Cr(2)−C(47)	99.23(9)
Cr(3)−C(32)	2.267(2)	N(2)−Cr(2)−C(13)	87.33(8)
Cr(3)−C(47)	2.231(3)	C(32)−Cr(2)−C(13)	157.38(8)
Cr(3)−C(62)	2.275(2)	C(47)−Cr(2)−C(13)	94.82(9)
Cr(4)−N(3)	2.0531(18)	N(3)−Cr(3)−C(47)	81.16(8)
Cr(4)−N(4)	1.9703(18)	N(3)−Cr(3)−C(32)	161.06(8)
Cr(4)−C(62)	2.159(2)	C(47)−Cr(3)−C(32)	97.53(9)
		N(3)−Cr(3)−C(62)	95.96(8)
		C(47)−Cr(3)−C(62)	159.67(10)
		C(32)−Cr(3)−C(62)	91.56(8)
		N(4)−Cr(4)−N(3)	167.09(8)
		N(4)−Cr(4)−C(62)	82.21(9)
		N(3)−Cr(4)−C(62)	100.9(8)

methylene moiety, which bridges to an inner chromium. In addition, a THF molecule binds to Cr(1) to afford three four-coordinate chromiums {Cr(1), Cr(2), and Cr(3)} and one three-coordinate (Cr(4)) metal. For the latter, the interligand angles are 167.14(8)°, 100.45(8)°, and 82.27(8)°, consistent with a distorted T-shaped geometry. Such a coordination mode is unusual for chromium and has only been found in a handful of complexes.[52,53] The two inner chromium atoms, Cr(2) and Cr(3), are each coordinated to one bridging amide ligand and three methylene moieties that bridge to the outer metals. The coordination modes of Cr(2) and Cr(3) are consistent with distorted square planar geometries (the interligand angles for Cr(2) are N(2)−Cr(2)−C(13) 87.33(8)°, N(2)−Cr(2)−C(32) 79.99(8)°, C(13)−Cr(2)−C(47) 94.82(9)°, and C(32)−Cr(2)−C(47) 99.23(9)°; for Cr(3) they are N(3)−Cr(3)−C(47) 81.16(8)°, N(3)−Cr(3)−C(62) 95.96(8)°, C(32)−Cr(3)−C(62) 91.56(8), and C(32)−Cr(3)−C(47) 97.53(9)°). The terminal metal amido distances to Cr(1) (1.990(2) Å) and Cr(2) (1.971(2) Å) lie between those observed in $Cr\{N(SiMe_3)_2\}_2(THF)_2$ (Cr−N = 2.09(1) Å)[54] and in the dimers $R_2NCr(\mu\text{-}NR_2)_2CrNR_2$ (R = Pr^i and Cy) (Cr−N = 1.927(3) and 1.942(7) Å)[55] and are close to the distance of 1.996(1) Å found in $Cr\{N(H)Ar^{Pr^i_6}\}_2$ ($Ar^{Pr^i_6}$ = C_6H_3-2,6(C_6H_2-2,4,6-Pr^i_3)$_2$).[7] The bridging Cr−N metal amido distances resemble those found in other Cr(II) bridged amido complexes.[55,56] The Cr−C bond lengths (2.159(2)−2.275(2) Å) are longer than the 2.08(1) Å observed in $Cr(Mes)_2(THF)_2$ (Mes = C_6H_2-2,4,6-Me_3), $Cr(Mes)_2$(bipyridyl) (Cr−C = 2.168(4) Å),[57] $Cr(CH_2SiMe_3)_2$(dippe)[58] (Cr−C = 2.131(2) Å), or $CrMe_2(dmpe)_2$,[59] perhaps as a result of their bridging nature in **4**. The Cr(2)···Cr(3) and Cr(3)···Cr(4) distances, 2.727 and 2.662 Å, respectively, are longer than twice the single bond radius of Cr (2.44 Å).[60] The Cr(1)···Cr(2) distance (2.371 Å) is about 0.3 Å shorter than the Cr(2)···Cr(3) and Cr(3)···Cr(4) distances, presumably because of the coordination of THF, resulting in the increase of steric effect, "pushing" Cr(1) inward. Interestingly, the stoichiometry of **4** shows that the ratio of Cr to amido ligand is 1:1. However, the reaction of $CrCl_2(THF)_2$ and LiN(Dipp)$SiMe_3$ did not result in the isolation of any crystalline product.

Magnetic Properties. For $Fe\{N(SiMe_3)Dipp\}_2$, **1**, the temperature dependence of $\chi_M T$ and $1/\chi_M$ obtained between 5 and 300 K in an applied field of 0.01 T is shown in Figure 3;

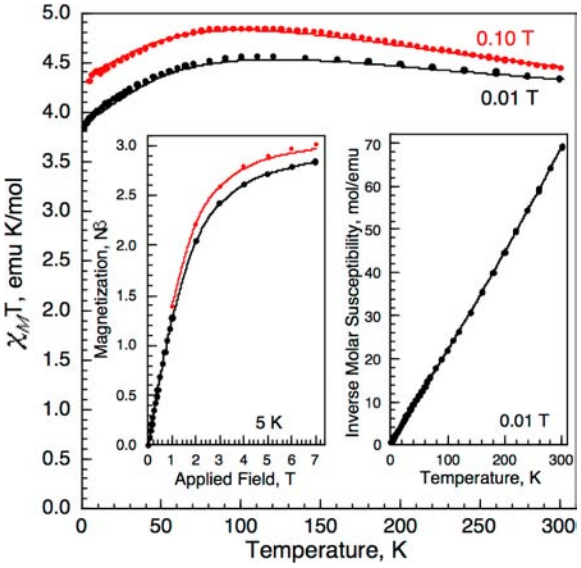

Figure 3. The temperature dependence of $\chi_M T$ obtained between 2 and 300 K in an applied field of 0.01 T, in black, and 0.1 T, in red, for **1**; the red data has been obtained from Figure 2 of ref 10. Right inset: The temperature dependence of $1/\chi_M$ obtained for **1** at 0.01 T. Left inset: The field dependence of the magnetization of **1** obtained at 5 K at 0.01 and 0.1 T. All the solid curves correspond to the fits obtained with PHI and discussed in the text.

the $\chi_M T$ obtained at 0.1 T of a separate preparation and study of **1** reported earlier[10] is also included in Figure 3 for comparison. Similar magnetic properties have been reported[3−5] for several somewhat similar linear two-coordinate iron(II) complexes.

It is apparent from Figure 3 either that $\chi_M T$ of **1** exhibits a small dependence on the applied field or that there are small differences in the samples used in this study and the earlier study.[61] At 0.01 T, $\chi_M T$ of **1** is observed to increase from 3.84 emu K/mol at 2 K to a maximum of 4.56 emu K/mol at 110 K and then to decrease to 4.34 emu K/mol at 300 K; the corresponding effective magnetic moment, μ_{eff}, increases from 5.41μ_B at 2 K to a maximum of 6.04μ_B at 110 K and then decreases to 5.89μ_B at 300 K. This behavior is typical[3−5,10,61] of a paramagnetic S = 2 iron(II) ion in a low-coordination environment that possesses a substantial spin−orbit coupling. The paramagnetic behavior is confirmed by the observed $1/\chi_M$ temperature dependence of **1**, a temperature dependence that is linear between 100 and 300 K.

The magnetization of **1** obtained at 5 K between 0 and 7 T is shown in black in the left inset to Figure 3. As expected, no hysteresis is observed at 5 K between ±7 T, and the slope of the initial magnetization agrees very well with the observed 5 K molar magnetic susceptibility. The magnetization, which is 2.83 Nβ at 7 T, is not saturated and is lower than the 4 Nβ that would be expected for a high-spin S = 2 iron(II) complex in the absence of any orbital contribution and any substantial single-ion magnetic anisotropy.

dx.doi.org/10.1021/ic402105m | Inorg. Chem. 2013, 52, 13584−13593

As noted above, the various experimental results shown in Figure 3 are typical of high-spin $S = 2$ iron(II) in a two coordinate environment in the presence of spin−orbit coupling. As a consequence, the $\chi_M T$ of **1** has been fit with the PHI code[62] to yield the best fits shown as the solid lines in Figure 3. The simultaneous fits with $S = 2$ and $L = 2$ of $\chi_M T$ obtained at 0.01 T between 2 and 300 K and the magnetization obtained at 5 K yields $B_2^0 = -117(1)$ cm^{-1}, $\lambda = -76(1)$ cm^{-1}, $g_{x,y} = 1.89(2)$, and $g_z = 1.78(1)$, where $B_k^q = B_2^0$ is the crystal field parameter, $A_k^q\langle r^k\rangle$, in the Steven's notation, λ is the spin−orbit coupling constant, and $g_{x,y}$ and g_z are the anisotropic electronic g-factors. The corresponding fit of $\chi_M T$ obtained at 0.1 T between 5 and 300 K and the magnetization obtained at 5 K yields $B_2^0 = -140(1)$ cm^{-1}, $\lambda = -90(1)$ cm^{-1}, $g_{x,y} = 1.74(2)$, and $g_z = 1.95(1)$. The details of the crystal field parameter and the specific Hamiltonian used in the fits may be found in the user manual provided with the PHI code.[62]

In the above fit, the $L = 2$ orbital contribution to the moment is required to fit the temperature dependence of $\chi_M T$ and is expected on the basis of the relative energies, $d_{xy} \approx d_{x^2-y^2} < d_{xz} \approx d_{yz} < d_{z^2}$, of the iron(II) 3$d$ orbitals in the linear coordination environment of **1** obtained from *ab initio* calculations.[61] These calculations yield nearly degenerate 3d_{xy} and 3$d_{x^2-y^2}$ orbitals at 0 and 164 cm^{-1}, a relatively small calculated orbital ground state splitting that facilitates an orbital contribution to the observed moment.

For a linear iron(II) coordination environment these fits clearly indicate the importance of both an extensive orbital contribution[10] as a consequence of spin−orbit coupling[63] within the electronic ground state of a complex such as **1**, and the associated extensive g-factor anisotropy, an anisotropy that has been predicted by Dai and Whangbo.[64]

The temperature dependence of $\chi_M T$ of Co{N(SiMe$_3$)-Dipp}$_2$, **2**, was measured, after zero-field cooling, in a field of 0.01 T upon warming from 2 to 300 K, see Figure 4. The inverse molar susceptibility of **2** is linear from 70 to 300 K and a linear fit, see the inset to Figure 4, yields a Weiss temperature of −5.8 K, a Curie constant, C, of 3.04 emu K/mol, a value that corresponds to a μ_{eff} of 5.93μ_B and $g = 2.54$ if $S = 3/2$. This behavior is very characteristic of a paramagnetic $S = 3/2$ cobalt(II) complex that has an $L = 2$ orbital contribution to its moment.

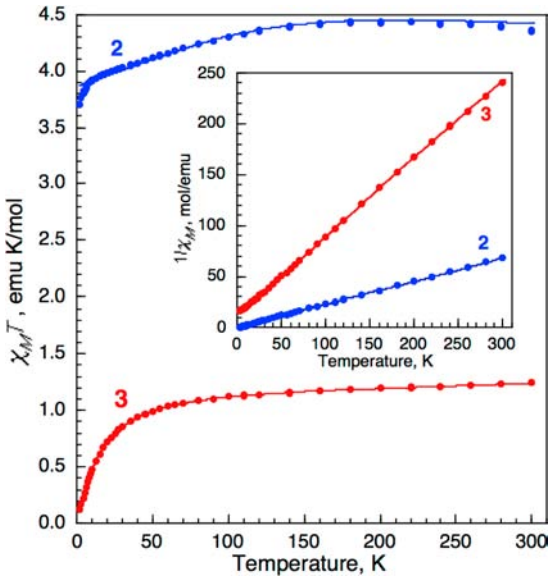

Figure 4. The temperature dependence of $\chi_M T$ obtained between 2 and 300 K in an applied field of 0.01 T, for **2**, in blue, and **3**, in red. For **2**, the solid lines correspond to a $\chi_M T$ fit between 10 and 300 K and for **3** a fit between 2 and 300 K with the parameters given in the text. Inset: the temperature dependence of $1/\chi_M$ and the corresponding fits between 2 and 300 K for **2** and **3**.

The $\chi_M T$ of **2** has been fit with the PHI code[62] to yield the best fits shown as the solid lines in Figure 4. The simultaneous fits with $S = 3/2$ and $L = 2$ of $\chi_M T$ obtained at 0.01 T between 10 and 300 K and the magnetization obtained at 5 K yields $B_2^0 = -161(1)$ cm^{-1}, $\lambda = -183(2)$ cm^{-1}, $g_{x,y} = 2.15(2)$, and $g_z = 2.37(1)$. The sharp decrease in $\chi_M T$ between 2 and 10 K is presumably the result of long-range antiferromagnetic exchange coupling between molecules of **2** and has not been included in the fit.

Because of the $L = 2$ orbital contribution to the moment required to fit the $\chi_M T$ of **2** there must be a different ordering of the five 3d orbitals in **2** compared with those of **1**; the ordering given for **1** above would not permit any orbital contribution in the case of the 3d^7 cobalt(II) electronic configuration. Thus, it seems quite likely that the 3d orbital ordering in **2** is at least similar to the ordering $d_{z^2} < d_{xy} \approx d_{x^2-y^2} < d_{xz} \approx d_{yz}$ that has been obtained[11] by *ab initio* calculations for the 3d^7 electronic configuration of the iron(I) ion in $[Fe(C(SiMe_3)_3)_2]^-$, anion. In this case, one of the three electrons in the virtually degenerate $d_{xy} \approx d_{x^2-y^2}$ orbitals will yield an $L = 2$ orbital moment in **2**.

The temperature dependence of $\chi_M T$ for Ni{N(SiMe$_3$)-Dipp}$_2$, **3**, was measured, after zero-field cooling, in a field of 0.01 T upon warming from 2 to 300 K, see Figure 4. The inset to this figure shows that the inverse molar susceptibility of **3** is linear from 50 to 300 K with a Weiss temperature of −15.8 K, a Curie constant, C, of 1.297 emu K/mol, a value that corresponds to an effective magnetic moment, μ_{eff}, of 3.22μ_B (cf. 2.67μ_B by the Evans' method in ref 17), and $g = 2.28$ if $S = 1$. This behavior is very characteristic of a paramagnetic nickel(II) complex exhibiting zero-field splitting that lowers $\chi_M T$ at low temperatures.

The $\chi_M T$ of **3** has been fit with the PHI code[62] to yield the best fits shown as the solid lines in Figure 4. The fit with $S = 1$ and $L = 0$ of $\chi_M T$ obtained at 0.01 T between 2 and 300 K yields $D = -67.5(5)$ cm^{-1}, $E = -9.17(10)$ cm^{-1}, $g = 2.13(1)$, and $\alpha = 0.000372$ emu/mol(1), where $N\alpha$ is the second-order Zeeman contribution to the paramagnetic molar susceptibility. It is not possible to fit the $\chi_M T$ of **3** if $L = 2$ or 1.

In the case of **3**, the lack of any orbital contribution to the moment is consistent with the full occupation in a 3d^8 nickel(II) complex of the virtually degenerate $d_{xy} \approx d_{x^2-y^2}$ orbitals where the relative ordering[53] of the 3d orbitals is $d_{z^2} < d_{xy} \approx d_{x^2-y^2} < d_{xz} \approx d_{yz}$, that is, essentially the same as noted above for the cobalt(II) complex, **2**.

Finally, a summary plot of the temperature dependence of the effective moments for **1**−**3**, under an applied field of 0.01 T, is presented in Figure 5. This plot illustrates the large difference in orbital moments between nickel (**3**) and iron (**1**) or cobalt (**2**) species; clearly, the values for **1** and **2** are significantly larger than the $g = 2$ spin-only μ_{eff} values of 4.90μ_B and 3.87μ_B expected for high spin complexes. In contrast, the μ_{eff} for Ni(II) in **3** also exceeds the spin-only value of 2.83μ_B, but the difference, 0.32μ_B, is smaller than the 1.06μ_B and 1.91μ_B observed for **1** and **2**, respectively.

dx.doi.org/10.1021/ic402105m | *Inorg. Chem.* 2013, 52, 13584−13593

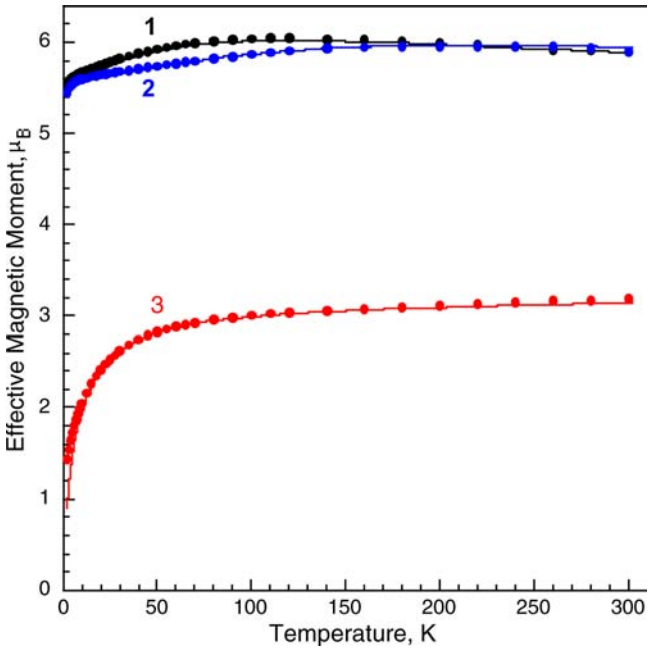

Figure 5. The temperature dependence of the effective magnetic moments for **1**−**3** obtained at 0.01 T and the corresponding fits shown in Figures 3 and 4

For $[Cr\{N(SiMe_2CH_2)Dipp\}_2Cr]_2(THF)$ (**4**), the temperature dependence of $\chi_M T$, obtained after zero-field cooling between 2 and 300 K in an applied field of 0.01 T, and the field dependence of the 5 K magnetization are both shown in Figure 6.

It is apparent that both $\chi_M T$ and the 5 K magnetization values are very small for a complex containing four chromium(II) ions, presumably because of extensive antiferromagnetic

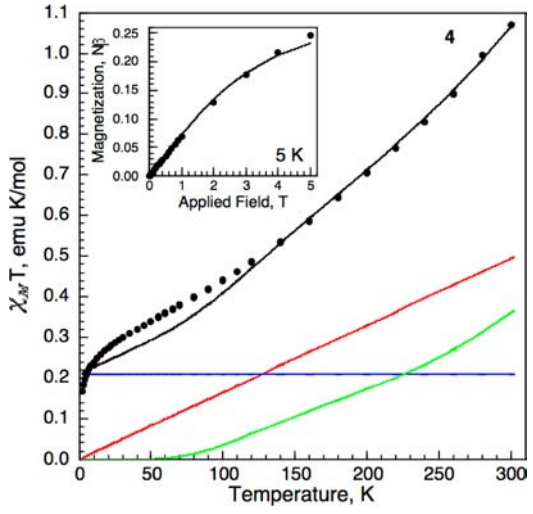

Figure 6. The temperature dependence of $\chi_M T$ obtained between 2 and 300 K at 0.01 T of $[Cr\{N(SiMe_2CH_2)Dipp\}_2Cr]_2(THF)$, **4**. The black line is the calculated $\chi_M T$, the green line is the contribution from exchange coupling among the four cations in terms of the parameters given in the text, the red line corresponds to *Na*, the temperature independent paramagnetic susceptibility, and the blue line corresponds to the presence of 7 wt % of a paramagnetic chromium(II) impurity with $S = 2$ and $g = 2$. Inset: the magnetization of **4** obtained at 5 K and its fit with the same parameters as used for $\chi_M T$.

exchange coupling between them. As a result PHI[61] has been used to simultaneously simulate the $\chi_M T$ and the 5 K magnetization of **4** yielding the solid lines shown in Figure 6. Because of the presence of four crystallographically distinct chromium(II) ions and the extensive correlation between the parameters given below, it has proven impossible to do a refinement of the parameters, and the resulting simulation has not been completely optimized. Further, the calculated values assume that there is no change in the structure of **4** as a function of temperature, changes that could add a small temperature dependence to the exchange coupling.

Based on the structure of **4** presented above, the magnetic exchange coupling has been modeled in terms of five exchange coupling constants, J_i, with an isotropic Heisenberg exchange coupling Hamiltonian, $\mathbf{H} = -2J\mathbf{S}_1\cdot\mathbf{S}_2$, with $g = 2$ and $S = 2$. The five parameters correspond to antiferromagnetic exchange coupling of $J_1 = -270$ cm^{-1} between Cr(1) and Cr(2), $J_2 = -220$ cm^{-1} between Cr(3) and Cr(4), $J_3 = -80$ cm^{-1} between Cr(2) and Cr(3), and ferromagnetic coupling of $J_4 = 20$ cm^{-1} between Cr(2) and Cr(4) and $J_5 = 28$ cm^{-1} between Cr(1) and Cr(3). Thus, the five coupling constants are in the order $J_1 < J_2 < J_3 < J_4 < J_5$, an order which is consistent with the exchange coupling pathways and distances in **4**. In addition, the simulation required the contribution of a temperature-independent paramagnetic susceptibility, *Na*, of 0.001650 emu/mol or an average of 0.000412 emu/mol of chromium(II) ions. Finally, in order to fit the ca. 0.2 emu K/mol $\chi_M T$ values at the very lowest temperatures, one must include a trace of paramagnetic impurity. If this impurity is a chromium(II) ion with $S = 2$ and $g = 2$, then it corresponds to ca. 7 wt % of the sample. Finally, it should be noted that all attempted simulations with $S = 2$ for Cr(1) and Cr(4) and $S = 1$ for Cr(2) and Cr(3) failed.

Although the magnitudes of J_1 and J_2 are rather larger than one might expect for exchange coupling, the large negative values are required to yield the very low high temperature $\chi_M T$ values observed for **4**. Also it should be noted that in **4** there are two superexchange pathways and a 2.371 Å direct exchange pathway between Cr(1) and Cr(2) and two superexchange pathways and a 2.662 Å direct exchange pathway between Cr(3) and Cr(4), pathways which in combination can yield strong antiferromagnetic exchange. In contrast, there are two superexchange pathways but a longer 2.727 Å direct exchange pathway between Cr(2) and Cr(3). For comparison, the related trinuclear chromium(II) complex,[11] $Cr\{Ar^{Pr^i_4}Cr(\mu\text{-}NMe_2)_2\}_2$, also has two superexchange pathways between the two equivalent terminal Cr(1) sites and the central Cr(2) site, but a direct exchange distance of 2.9515(3) Å and, as a consequence, a less negative Cr(1) to Cr(2) exchange coupling constant of −47(1) cm^{-1}.

Spectroscopy and Bonding. In order to further investigate the bonding and electronic spectra in complexes **1**−**3**, calculations were carried out using density functional theory.

The optimized geometries for the gas phase stuctures of **1**−**3** are illustrated in Figure 7. The calculated and experimental data display good agreement with less than a 2% difference between them. The eclipsed configuration of the ligands and linear geometries were calculated to be lowest in energy in all cases. The similarity of the calculated and experimental structures indicate that packing forces play little role in determining the details of the structure. The calculations also show the

dx.doi.org/10.1021/ic402105m | *Inorg. Chem.* 2013, 52, 13584−13593

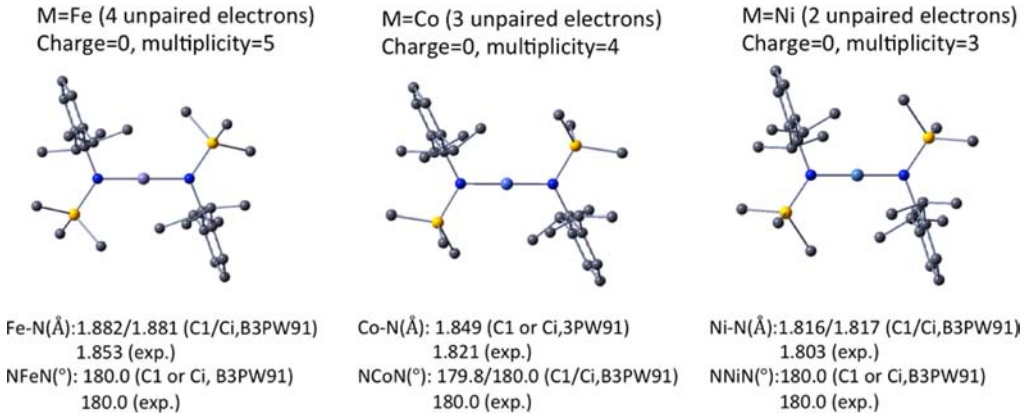

Figure 7. Calculated geometries of **1**−**3** at B3PW91//6-311+G* (M)/6-31G(d) (other atoms) level of optimization.

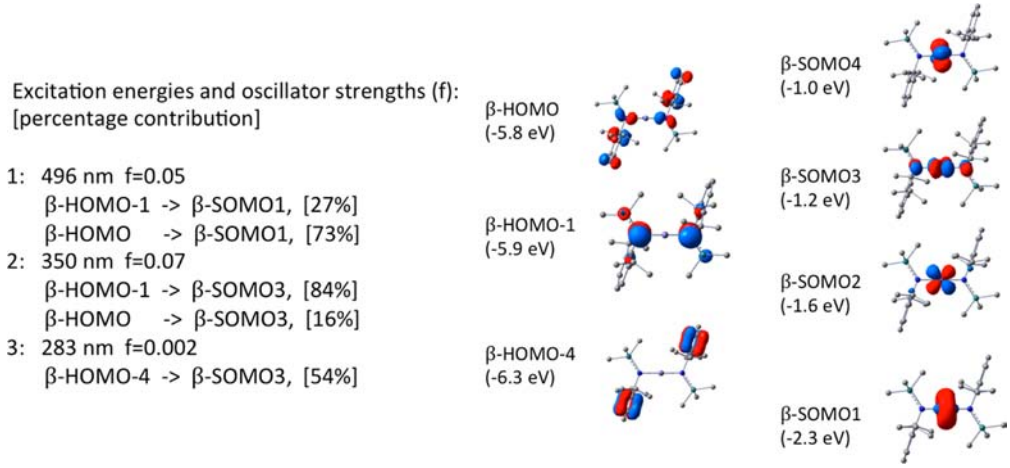

Figure 8. Excitation energies and oscillator strengths for $Fe\{N(SiMe_3)Dipp\}_2$, **1**. Calculated by the TD-B3PW91 method.

Table 5. Dispersion Effects for 1 (Fe complex), 2 (Co complex), and 3 (Ni complex) with C_1 and C_i Symmetry

	M = Fe					M = Co					M = Ni				
	calcd					calcd					calcd				
	B3PW91		B3PW91-D3		expt	B3PW91		B3PW91-D3		expt	B3PW91		B3PW91-D3		expt
	C_1	C_i	C_1	C_i	C_i	C_1	C_i	C_1	C_i	C_i	C_1	C_i	C_1	C_i	C_i
M−N (Å)	1.882	1.881	1.866	1.865	1.853	1.849	1.849	1.829 1.835	1.830	1.818	1.816	1.817	1.796 1.798	1.797	1.803
N−C (Å)	1.427	1.427	1.419	1.419	1.429	1.427	1.427	1.421 1.422	1.421	1.429	1.424	1.424	1.417 1.415	1.416	1.433
N−Si (Å)	1.758	1.758	1.745	1.746	1.726	1.761	1.762	1.756 1.748	1.751	1.731	1.762	1.763	1.751 1.746	1.748	1.742
N−M−N (deg)	180.0	180.0	180.0	180.0	180.0	179.8	180.0	175.0	180.0	180.0	180.0	180.0	177.9	180.0	180.0

absorptions in their electronic spectra are primarily due to electron transfer from various ligand-based N(p) or π-orbitals to metal d-orbitals or from metal d-orbitals to π^*-ligand orbitals. For example, the experimental spectrum of **1** displayed moderately intense absorptions at 467, 349, and 280 nm. The calculated absorptions were at 496, 350, and 283 nm, in good agreement with the observed values. These three absorptions originate in N(p)/aryl $\pi^* \rightarrow d_{z^2}$, N(p)/aryl $\pi^* \rightarrow d_{xz}$, and d_{xz}, $d_{yz} \rightarrow \pi^*$, aryl $\pi \rightarrow d_{xz}$ excitations, shown in Figure 8. Similar calculations for **2** and **3** afforded bands at 541, 504, and 284 nm for **2**, and at 652, 501, and 347 nm for **3**. The experimental spectrum for the cobalt species **2** reveals a very broad unresolved absorption (see Supporting Information) between 250 and 700 nm, possibly as a result of spin-orbit coupling. The spectrum for **3** reveals a shoulder absorption near 640 nm and an absorption at 510 and 345 nm, in good agreement with calculations.

The IR spectra of **1**, **2**, and **3** were calculated to yield several bands in the range ca. 100−900 cm^{-1} that are associated with the vibrations of the MN_2 core units. The experimental IR spectra of **1**−**3** are very similar (see Supporting Information). The bands observed below 650 cm^{-1} are relatively weak, and this is in agreement with the calculated absorptions (see Supporting Information). Thus, the symmetric M−N vibrations for **1**, **2**, and **3** were calculated to be in the range 374−382 cm^{-1}. Experimentally, a weak band near 410 cm^{-1} was observed

dx.doi.org/10.1021/ic402105m | Inorg. Chem. 2013, 52, 13584−13593

Table 6. Calculations of the Bond Dissociation Energies of 1−3 (C_i symmetry) at the B97D and B3PW91 Levels with and without Dispersion Corrections

	BDE/E_{disp} (kcal mol^1)				
	real-system model				isomer (bent)
	M = Fe	M = Co	M = Ni		M = Ni
B3PW91	68.3	63.8	59.1	55.1[a]	52.6[a]
B3PW91-D3	89.9/21.6	84.9/21.1	83.7/24.6	79.0[a]/23.9[a]	76.3[a]/23.7[a]
B97D	87.0/26.2	80.2/28.5	77.5/29.4	-	74.1/29.2

[a]Energies are BSSE-corrected.

for each compound (see Supporting Information for spectra). The asymmetric M−N stretching bands were calculated to be more intense and more energetic, with the most intense being calculated to be near 900 cm^{-1}. Complexes **1**, **2**, and **3** exhibited relatively strong absorptions at 910, 910, and 905 cm^{-1} respectively.

Dispersion Effects. To estimate the extent of dispersion effects, the geometries of **1**, **2**, and **3** were reoptimized at the B3PW91-D3 level. The corresponding data are included in Tables 5 and 6. We found that the M−N bond lengths become slightly shorter after the dispersion correction, due to dispersive attractive forces involving the bulky substituents on the N atoms, which can strongly stabilize the complex by transmetallic C−H···H−C interactions that afford a dispersion stabilization in the range 21.1−29.6 kcal mol^{-1}. This perhaps surprising range of energies is, however, consistent with those calculated by Ziegler for the species $Ar^{Pr^i_4}CrCrAr^{Pr^i_4}$ ($Ar^{Pr^i_4}$ = C_6H_3-2,6(C_6H_3-2,6-Pr^i_2)$_2$).[38]

The extent of the dispersive force contribution to the M−N bond energy was obtained by calculating the energy of the optimized structure and subtracting the calculated energies with and without the inclusion of dispersion correction of the molecular fragments A ({(Me_3Si)Dipp}N−M) and B ({−N-($SiMe_3$)Dipp}) resulting from cleavage of the M−N bond, as illustrated in Table 6. The B97D data afford stabilizations that differ only by ca. 6 kcal/mol from the B3PW91-D3 data, suggesting that the B97D functional can efficiently predict the trends in the dispersion energy, even if it tends to underestimate such energies slightly. A similar treatment for M{N($SiMe$)$_2$}$_2$ in Figure S13, Supporting Information or M{N(SiH_3)$_2$}$_2$ in Figure S14, Supporting Information, show lower dispersion stabilization energies of *ca.* 12 or *ca.* 5 kcal mol^{-1} respectively, consistent with decreasing numbers of interactions.

To explore the feature of coplanarity of the two NSiC planes in **1**−**3**, we took the Ni complex **3** as an example to draw a plot of total energy vs the angle of these two planes at the B97D level (Figure S11, Supporting Information). The plot exhibits two minima: a global minimum for the real-system model and a local minimum with an angle of 120° between the planes. The fully optimized isomer with a bent NNiN angle in Table 6 corresponds to the local minimum. It is noteworthy that the isomer with the dihedral angle around 50° between the planes of the two amido substituents is less stable by 2.5 kcal/mol (B3PW91 with BSSE) or 2.7 kcal/mol (B3PW91-D3 with BSSE) than the Ni real-system model, but their dispersion energies are similar. Therefore, it can be concluded that dispersion effects are not the key determinant for this angular feature.

The linear geometry has also been confirmed by the density functional theory at B3PW91 and B97D levels carried out with a simple model system in which the $SiMe_3$ and isopropyl groups are replaced by SiH_3 and H in Figure S12, Supporting Information. In marked contrast to the real-system model, which is the global minimum energy conformation, the analogous and simple model with C_{2h} symmetry gives only ca. 5 kcal/mol of dispersion energy at B97D level and is less stable than that with the planar core atoms, suggesting that electronic and steric effects from bulky substituents also play an important role in the real-system model. The results show that the NMN angle is always nearly 180°, whether or not the two amido substituents are coplanar.

CONCLUDING REMARKS

To summarize, the synthesis of three transition metal complexes containing a rigorously linear N−M−N (M = Fe−Ni) array was effected by treatment of the corresponding metal chloride with 2 equiv of LiN($SiMe_3$)Dipp. In addition, the tetranuclear species [Cr{N($SiMe_2CH_2$)Dipp}$_2$Cr]$_2$(THF) was obtained by a similar reaction. The two-coordinate iron and cobalt derivatives exhibit high effective magnetic moments due to in-state or out-of-state orbital magnetism. DFT calculations modified to include dispersion effects show that these effects play a key role in stabilizing the structure. They also suggest that dispersion effects are present in many other sterically crowded transition metal complexes, but are generally unrecognized. The investigation of the use of the −N($SiMe_3$)Dipp and related ligands to stabilize other low coordinate transition metal species is in hand.

ASSOCIATED CONTENT

Supporting Information

CIF files for **1**−**4**, electronic spectra of **1**−**3**, calculated electronic transitions for **1**−**3**, IR spectra for **1**−**3** in the 200−1500 cm^{-1} region, calculated M−N vibrational bands, calculated BDEs and ΔE_{disp} for **3**, with changes in the rotation angle between the nitrogen coordination planes, calculated structures of the model species M{N(SiH_3)Ph}$_2$ (M = Fe, Co, or Ni), calculations of the BDEs of M{N($SiMe_3$)$_2$}$_2$ and M{N(SiH_3)$_2$}$_2$, and a complete citation for ref 24. This material is available free of charge via the Internet at http://pubs.acs.org.

AUTHOR INFORMATION

Corresponding Authors

*E-mail: pppower@ucdavis.edu.
*E-mail: nagase@ims.ac.jp.
*E-mail: glong@mst.edu.

Notes

The authors declare no competing financial interest.

■ ACKNOWLEDGMENTS

We thank the National Science Foundation (Grant No. CHE-1263760) and a Grant-in-Aid for Specially Promoted Research (Grant No. 22000009) from MEXT of Japan for support of this work. The authors thank Dr. J. Zadrozny for providing the data on complex **1** obtained at 0.10 T.

■ REFERENCES

(1) Viefhaus, T.; Schwarz, W.; Hübler, K.; Locke, K.; Weidlein, J. *Z. Anorg. Allg. Chem.* **2001**, *627*, 715.
(2) LaPointe, A. M. *Inorg. Chim. Acta* **2003**, *345*, 359.
(3) Reiff, W. M.; LaPointe, A. M.; Witten, E. H. *J. Am. Chem. Soc.* **2004**, *126*, 10206.
(4) Reiff, W. M.; Schulz, C. E.; Whangbo, M.-H.; Seo, J. I.; Lee, Y. S.; Potratz, G. R.; Spicer, C. W.; Girolami, G. S. *J. Am. Chem. Soc.* **2009**, *131*, 404.
(5) Merrill, W. A.; Stich, T. A.; Brynda, M.; Yeagle, G. J.; Fettinger, J. C.; de Hont, R.; Reiff, W. M.; Power, P. P. *J. Am. Chem. Soc.* **2009**, *131*, 12693.
(6) (a) Bryan, A. M.; Merrill, W. A.; Fettinger, J. C.; Reiff, W. M.; Power, P. P. *Inorg. Chem.* **2012**, *51*, 3366. (b) Li, E. J.; Song, H.; Cui, C.; Cheng, J.-P. *Inorg. Chem.* **2008**, *47*, 3468.
(7) Boynton, J. N.; Merrill, W. A.; Fettinger, J. C.; Reiff, W. M.; Power, P. P. *Inorg. Chem.* **2012**, *51*, 3212.
(8) Bŏca, R. *Coord. Chem. Rev.* **2004**, *248*, 757.
(9) Neese, F.; Pantazis, D. A. *Faraday Discuss.* **2011**, *148*, 229.
(10) Zadrozny, J.; Atanasov, M.; Bryan, A. M.; Lin, C.-Y.; Rekken, B. D.; Power, P. P.; Neese, F.; Long, G. J. *Chem. Sci.* **2013**, *4*, 125.
(11) Zadrozny, J. M.; Xiao, D. J.; Atanasov, M.; Long, J. R.; Grandjean, F.; Neese, F.; Long, J. R. *Nat. Chem.* **2013**, *5*, 577.
(12) (a) Power, P. P. *Chem. Rev.* **2012**, *112*, 3482. (b) Kays, D. L. *Dalton Trans.* **2011**, *40*, 769.
(13) Power, P. P. *J. Organomet. Chem.* **2004**, *689*, 3904.
(14) Buttrus, N. H.; Eaborn, C.; Hitchcock, P. B.; Smith, J. D.; Sullivan, A. C. *J. Chem. Soc., Chem. Commun.* **1985**, 1380.
(15) Nguyen, T.; Panda, A.; Olmstead, M. M.; Richards, A. F.; Stender, M.; Brynda, M.; Power, P. P. *J. Am. Chem. Soc.* **2005**, *127*, 8545.
(16) (a) Chao, Y.-W.; Wexler, P. A.; Wigley, D. E. *Inorg. Chem.* **1989**, *28*, 3860. (b) Vargas, W.; Englich, U.; Ruhlandt-Senge, K. *Inorg. Chem.* **2002**, *41*, 5602. (c) Schumann, H.; Gottfriedsen, J.; Dechert, S.; Girgsdies, F. *Z. Anorg. Allg. Chem.* **2000**, *626*, 747.
(17) Lipschutz, M. I.; Tilley, T. D. *Chem. Commun.* **2012**, *48*, 7146.
(18) Kennepohl, D. K.; Brooker, S.; Sheldrick, G. M.; Roesky, H. W. *Chem. Ber.* **1991**, *124*, 2223.
(19) Job, R.; Earl, R. *Inorg. Nucl. Chem. Lett.* **1979**, *15*, 81.
(20) Ward, L. G. L. *Inorg. Synth.* **1971**, *13*, 154.
(21) SADABS, an empirical absorption correction program for the SAINT-Plus-NT, version 5.0, Bruker AXS, Madison, WI, 1998.
(22) (a) SHELXTL, version 5.1, Bruker AXS, Madison, WI, 1998. (b) Dolomanov, O. V.; Bourkis, L. J.; Gilder, R. J.; Howard, J. A. K.; Puschmann, H. *J. Appl. Cryst.* **2009**, *42*, 339.
(23) Bain, G. A.; Berry, J. F. *J. Chem. Educ.* **2008**, *85*, 532.
(24) Frisch, M. J. et al. Gaussian 03 (Revision E.01) and 09 (Revision D.01). Gaussian, Inc.: Wallingford, CT. 2004. For full citations, see Supporting Information.
(25) (a) Grimme, S.; Antony, J.; Ehrlich, S.; Krieg, H. *J. Chem. Phys.* **2010**, *132*, 154104. (b) Boys, S. F.; Bernardi, F. *Mol. Phys.* **1970**, *19*, 553.
(26) Bürger, H.; Wannagat, U. *Monatsh.* **1964**, *95*, 1099.
(27) Andersen, R. A.; Faegri, K.; Green, J. C.; Haaland, A.; Lappert, M. F.; Leung, W.-P.; Rypdal, K. *Inorg. Chem.* **1988**, *27*, 1782.
(28) Bryan, A. M.; Long, G. J.; Grandjean, F.; Power, P. P. *Inorg. Chem.* **2013**, *52*, 12152.
(29) Bartlett, R. A.; Chen, H.; Power, P. P. *Angew. Chem., Int. Ed.* **1989**, *28*, 316.
(30) Chen, H.; Bartlett, R. A.; Olmstead, M. M.; Power, P. P.; Shoner, S. C. *J. Am. Chem. Soc.* **1990**, *112*, 1048.
(31) Hope, H.; Olmstead, M. M.; Murray, B. D.; Power, P. P. *J. Am. Chem. Soc.* **1985**, *107*, 712.
(32) Laskowski, C. A.; Hillhouse, G. L. *J. Am. Chem. Soc.* **2008**, *130*, 13846.
(33) Bartlett, R. A.; Power, P. P. *J. Am. Chem. Soc.* **1987**, *109*, 7563.
(34) Chen, H.; Bartlett, R. A.; Dias, H. V. R.; Olmstead, M. M.; Power, P. P. *J. Am. Chem. Soc.* **1989**, *111*, 4338.
(35) Ni, C.; Power, P. P. *Chem. Commun.* **2009**, *37*, 5543.
(36) Ni, C.; Stich, T. A.; Long, G. J.; Power, P. P. *Chem. Commun.* **2010**, *38*, 4466.
(37) Takagi, N.; Schmidt, M. W.; Nagase, S. *Organometallics* **2001**, *20*, 1646.
(38) Ndambuki, S.; Ziegler, T. *Inorg. Chem.* **2012**, *51*, 7794.
(39) Schreiner, P. R.; Chernish, L. V.; Gunchenko, P. A.; Tikhonchuk, E. Y.; Hausmann, H.; Serafin, M.; Schlecht, S.; Dahl, J. E. P.; Carlson, R. M. K.; Fokin, A. A. *Nature* **2011**, *477*, 308.
(40) Au-Yeung, H. Y.; Lam, C. H.; Lam, C.-K.; Wang, W. Y.; Lee, H. K. *Inorg. Chem.* **2007**, *46*, 7695.
(41) (a) Bradley, D. C.; Hursthouse, M. B.; Malik, K. M. A.; Möseler, R. *Transition Met. Chem.* **1978**, *3*, 253. (b) Murray, B. P.; Power, P. P. *Inorg. Chem.* **1984**, *23*, 4584.
(42) Olmstead, M. M.; Power, P. P.; Shoner, S. C. *Inorg. Chem.* **1991**, *30*, 2547.
(43) Bennett, C. R.; Bradley, D. C. *J. Chem. Soc., Chem. Commun.* **1974**, 29.
(44) Simpson, S. J.; Andersen, R. A. *Inorg. Chem.* **1981**, *20*, 3627.
(45) Planalp, R. P.; Andersen, R. A.; Zalkin, A. R. *Organometallics* **1983**, *2*, 16.
(46) Berno, P.; Gambarotta, S. *Organometallics* **1994**, *13*, 2569.
(47) Putzer, M. A.; Magull, J.; Goesmann, H.; Neumüller, B.; Dehnicke, K. *Chem. Ber.* **1996**, *129*, 1401.
(48) Simpson, S. J.; Turner, H. W.; Andersen, R. A. *Inorg. Chem.* **1981**, *20*, 2991.
(49) Messere, R.; Spirlet, M.-R.; Jan, D.; Demonceau, A.; Noels, A. F. *Eur. J. Inorg. Chem.* **2000**, 1151.
(50) Damhus, T.; Pedersen, E. *Inorg. Chem.* **1984**, *23*, 695.
(51) Bino, A.; Johnston, D. C.; Goshorn, P. P.; Halbert, T.; Stiefel, E. I. *Science.* **1988**, *241*, 1479.
(52) Hvoslef, J.; Hope, H.; Murray, B. D.; Power, P. P. *J. Chem. Soc., Chem. Commun.* **1983**, 1438.
(53) Ni, C.; Long, G. J.; Grandjean, F.; Power, P. P. *Inorg. Chem.* **2009**, *48*, 11594.
(54) Bradley, D. C.; Hursthouse, M. B.; Newing, C. W.; Welch, A. J. *J. Chem. Soc., Chem. Commun.* **1972**, 567.
(55) Kamalesh, B. P. R.; Feghali, K.; Kovacs, I.; Apana, K.; Gambarotta, S.; Yap, G. A. P.; Bensimon, C. *Dalton Trans.* **1998**, 1595.
(56) Lappert, M. F.; Power, P. P.; Protchenko, A.; Seeber, A. *Medal Amide Chemistry*; Wiley: Chichester, U.K., 2009; Chapter 6.
(57) Edema, J. J. H.; Gambarotta, S.; van Bolhuis, F.; Smeets, W. J. J.; Spek, A. L.; Chiang, M. Y. *J. Organomet. Chem.* **1990**, *389*, 47.
(58) Hermes, A. R.; Morris, R. J.; Girolami, G. S. *Organometallics* **1988**, *7*, 2372.
(59) Girolami, G. S.; Wilkinson, G.; Galas, A. M. R.; Thornton-Pett, M.; Hursthouse, M. B. *J. Chem. Soc., Dalton Trans.* **1985**, 1339.
(60) Pyykkö, P.; Atsumi, M. *Chem.—Eur. J.* **2009**, *15*, 186.
(61) Atanasov, M.; Zadrozny, J. M.; Long, J. R.; Neese, F. *Chem. Sci.* **2013**, *4*, 139.
(62) Chilton, N. F.; Anderson, R. P.; Turner, L. D.; Soncini, A.; Murray, K. S. *J. Comput. Chem.* **2013**, *34*, 1164.
(63) Kahn, O. *Molecular Magnetism*; Wiley-VCH: New York, 1993.
(64) Dai, D.; Whangbo, M.-H. *Inorg. Chem.* **2005**, *44*, 4407−4414.